J Mater Sci (2006) 41:6843–6854
DOI 10.1007/s10853-006-0953-3

Production of amorphous Fe–B alloy and α-Fe by chemical reduction of hematite using sodium borohydride

V. G. de Resende · G. M. da Costa · E. De Grave · L. Datas

Received: 13 May 2005 / Accepted: 7 December 2005 / Published online: 8 October 2006

Abstract Natural and well-crystallized hematite was suspended in water and treated at room-temperature (RT) with sodium borohydride in acid medium. The product of the reaction is a highly magnetic black powder, which is stable at RT. The $NaBH_4$ treatment converts about half of the hematite to an amorphous Fe–B alloy and to a small fraction of sub-micron sized, amorphous metallic-Fe nodules. Heating at 400 °C of this composite has resulted in the crystallization and/or oxidation of more than half of the amorphous Fe–B phase to α-Fe and Fe_3O_4 and B_2O_3, respectively. Further, the already present superficial, amorphous metallic Fe is converted to α-Fe and the original, plate like morphology of the hematite has changed to a mix of nodular and acicular particles. After treatment at 800 °C, the metallic Fe and the amorphous Fe–B have completely vanished, and the resulting product consists of hematite and $FeBO_3$ embedded in a matrix of α-Fe_2O_3.

V. G. de Resende · G. M. da Costa (✉)
Departamento de Química, Universidade Federal de Ouro Preto, Campus Universitário- Morro do Cruzeiro, Ouro Preto, MG 35400, Brazil
e-mail: magela@iceb.ufop.br

E. De Grave
Department of Subatomic and Radiation Physics, University of Ghent, Gent B-9000, Belgium

L. Datas
CIRIMAT (LCMIE), Université Paul Sabatier, Toulouse F-31062, France

Introduction

The use of sodium borohydride for the production of amorphous transition-metal boron alloys (TM-B) has been the subject of intense research in recent years [1–3]. This soft route offers several advantages with respect to other, more traditional methods (vapour deposition, melt spinning and sputtering, etc.) such as ease and promptness of the synthesis procedures and the possibility of preparing TM-B alloys with a broad variety in composition [4]. As far as it is known, all preparations methods reported so far in literature involve the addition of $NaBH_4$ to a solution containing the metallic ions. The effect of the pH, reaction time, and even of the sequence of the addition of the reactants on the composition and on the physicochemical properties of the obtained products have been examined by a number of authors [4–6]. On the other hand, the reaction of $NaBH_4$ with solid particles has not been investigated, and the main objective of this work is to report the formation of metallic iron in aqueous medium by the reduction of hematite particles.

This study is focused of the investigation of a new route for the production of amorphous Fe–B alloy and α-Fe by chemical reduction of well-crystallized hematite using sodium borohydride. Also, the stability of the products at high temperatures is studied by thermal treatment performed after the reduction with $NaBH_4$.

Experimental

The precursor (hereafter called EV) involved in this study is an iron ore concentrate sieved to below 46 μm and containing mainly hematite, with a small fraction of goethite.

About 1.2 g of the sample was dispersed in 200 ml of distilled water in which 4.0 g of $NaBH_4$ had been dissolved prior to the dispersion. Hydrochloric acid (100 ml, 0.20 M) was added dropwise under vigorous stirring. Four portions of 0.8 g each of $NaBH_4$ were added at regular intervals together with 100 ml of HCl. After 30 min of reaction, the solid was washed several times with distilled water and finally dried at 100 °C (sample BEV2). During the reaction the pH was found to remain more or less constant, varying between 9.6 and 10.2, whereas the temperature increased from room-temperature to 36.6 °C (Fig. 1).

Iron and boron contents were determined by titration with standard $K_2Cr_2O_7$ solution and ICP (Inductively Coupled Plasma), respectively, after dissolving the samples with concentrated HCl.

Thermal treatments in static air were performed during one hour at 400 °C (sample BEV2a) and 800 °C (BEV2b).

X-ray diffractograms (XRD) were recorded in the range 15–70° (2θ) with goniometer speed of 2°/min using a XRD-6000 Shimadzu diffractrometer equipped with a Co tube and Fe filter. Counts were registered every 0.02°.

Thermogravimetric curves between 25 °C and 1,200 °C were obtained under synthetic air (<3 ppm moisture, $O_2 + N_2 = 99.9\%$, $O_2 = 20.0 \pm 0.5\%$) with a flow of 50 ml/min using a Du Pont SDT 2960 apparatus and applying a heating rate of 20 °C/min. DSC measurements in the range 25–500 °C, heating rate of 10 °C/min and under an atmosphere of synthetic air (40 ml/min), were carried out with the powders contained in open aluminium pans.

Mössbauer spectra were collected with spectrometers operating at constant acceleration mode with triangular reference signals. $^{57}Co(Rh)$ sources were used. At room temperature, both conventional transmission Mössbauer spectroscopy (TMS spectra) and integral low-energy electron Mössbauer spectroscopy (ILEEMS spectra) have been applied. The latter variant probes the very top monolayers of the crystallites and gives information about those Fe species lying at distances of a few nanometers below the physical surfaces of the particles [7]. For samples BEV2 and BEV2a, TMS spectra were also recorded with the absorbers at a number of different temperatures between 12 K and RT. All Mössbauer spectra were computer-analysed in terms of model-independent distributions of hyperfine-parameter values and numerical data quoted hereafter refer to maximum probability values. Isomer shifts are referenced with respect to α-Fe at RT.

Finally, SEM and TEM images were provided by a Jeol electron microscope, with the powder samples dispersed in acetone. In particular, TEM was used to examine the microstructure of BEV2 and BEV2a in some detail. In addition to inspecting the TEM images, Selective Area Electron Diffraction (SAED) was applied to characterize the various entities observed in these images.

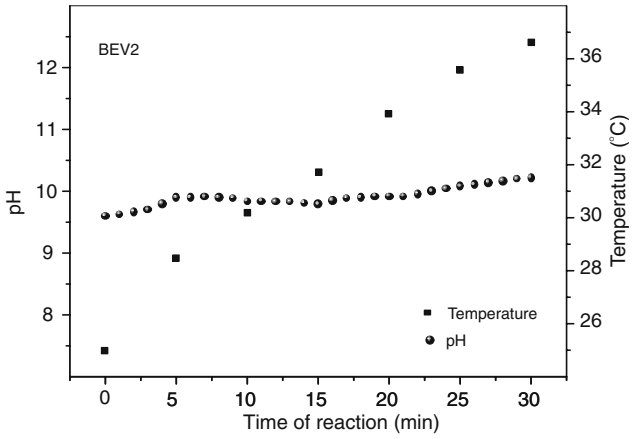

Fig. 1 Temperature and pH behaviour during the reaction of reduction of the hematite particles

Results and interpretation

Sample EV has the typical macroscopic appearance of an iron ore with specularity being the dominant Fe phase. Specularite is a variety of hematite characterized by aggregates of silvery, specular hematite flakes or tabular crystals and as such shows a metallic brilliance. Hematite is weakly ferromagnetic at RT and for this reason, it is only slightly attracted by a hand magnet. On the other hand, sample BEV2 is black and highly magnetic. The presence of ferric and/or ferrous ions that could eventually have been dissolved by the HCl was checked with potassium ferrocyanide ($K_4[Fe(CN)_6] \cdot 3H_2O$), but none of these ions were detected.

Figure 1 shows that the pH of the reaction medium slightly increases during the reduction of the specularite, probably because of the formation of hydroborate intermediates. Foster et al. [8] suggested that the reaction with borohydride proceeds via iron-hydroborate intermediates of the form $[(H_2O)_5Fe(HOBH_3)]^{2+}$. However, these intermediates have not yet been isolated because the reaction is extremely rapid. As the reaction proceeds the temperature smoothly increased from 25 °C to about 37 °C due to the exothermic character of this reaction.

At first glance, the XRD pattern of BEV2 only shows the peaks corresponding to well-crystallized hematite (Fig. 2), but a closer examination of the diffractogram (inset Fig. 2b) reveals the appearence of a shallow bump near 52° (2θ), a position that corresponds to the principal diffraction line α-iron. In addition, it can be noticed that the peaks corresponding to goethite (arrows in Fig. 2a) are not present in BEV2, indicating that this phase has completely reacted with the borohydride.

The TGA curve of EV (see Fig. 3) shows, in addition to a gradual weight loss spread out over the entire temperature range, a sudden drop near $T = 300$ °C. The corresponding DSC signal (also reproduced in Fig. 3) demonstrates that the sudden drop is an endothermic process. It can be attributed to the thermal decomposition of goethite, while the continuously decreasing mass is possibly due to removal of crystalline water molecules and/or remaining hydroxyl groups from the hematite structure.

On the other hand, the thermal analyses for sample BEV2 also reflect a continuous loss of mass (~1.9%) with increasing temperature, but only up to about $T = 400$ °C ($\Delta m \approx -1.9\%$), while in the range $T > 400$ °C two exothermic processes, associated with a multi-step gain in mass ($\Delta m \approx 10.2\%$), occur, indicating that some constituent of BEV2 reacts with the molecules of the surrounding atmosphere, which is synthetic air. Above 900 °C, again a continuously lowering in weight with increasing T is observed.

TMS and ILEEMS of sample EV at RT (Fig. 4) yield one sharp sextet of which the relevant Mössbauer parameters, i.e., hyperfine field H_{hf} and quadrupole shift $2\varepsilon_Q$ (see Table 1) are diagnostic of hematite. A very weak second sextet (area $S = 1\%$ relative to total spectral area) could be resolved from the TMS spectrum. Its hyperfine field and quadrupole shift at RT are 378 kOe and –0.26 mm/s, respectively, and can therefore be assigned to well-crystallized goethite, α-FeOOH [9].

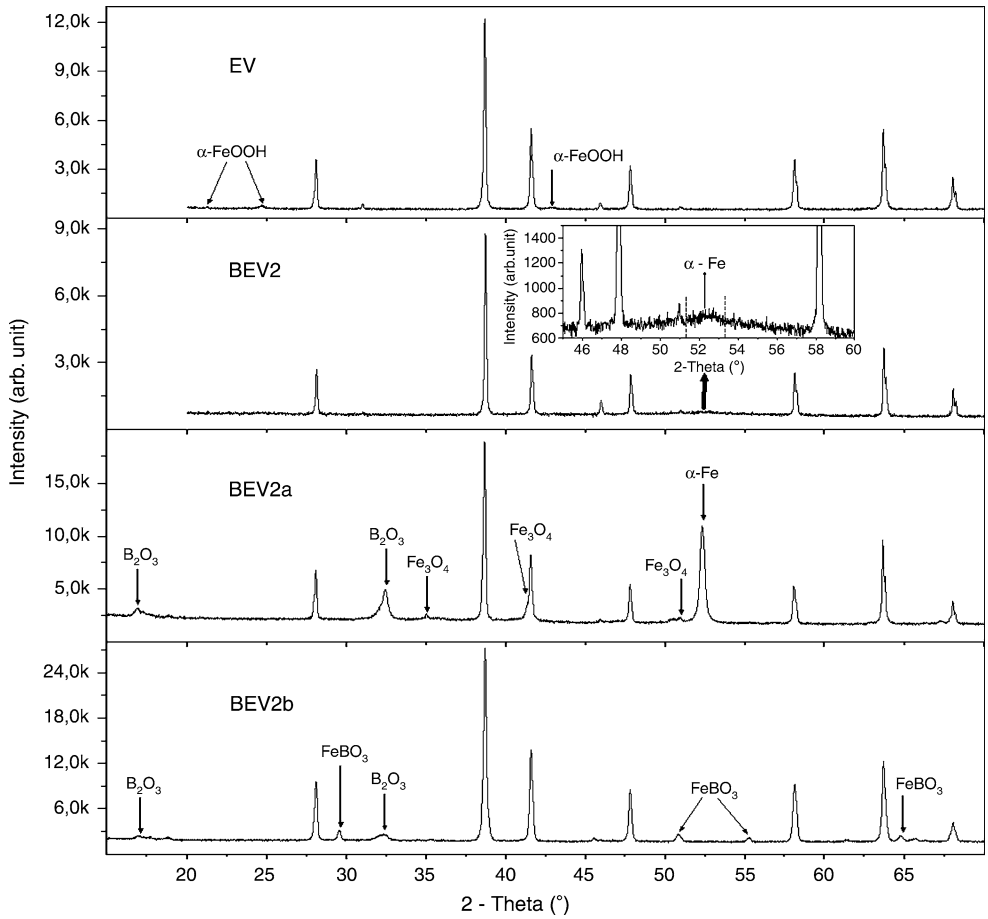

Fig. 2 X-ray diffraction patterns of the original iron ore (EV), and after treatment with borohydride (BEV2). Samples BEV2a and BEV2b were obtained by heating BEV2 at 400 °C and 800 °C, respectively

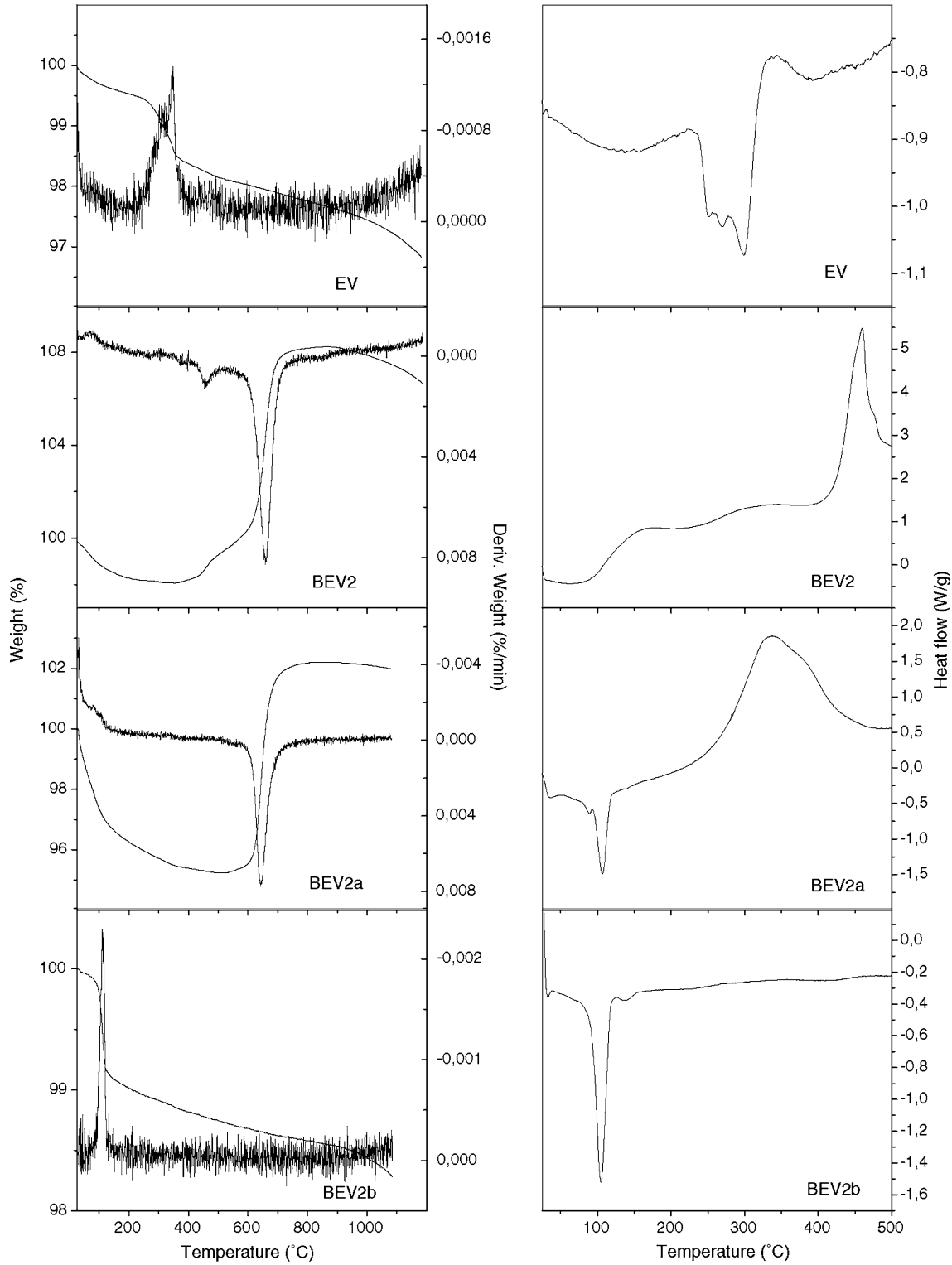

Fig. 3 Thermogravimetric curves (solid lines) and their respective derivatives (dotted lines, left side) and DSC curves (right side) of the studied samples

The RT TMS of sample BEV2 presents, in addition to the sharp hematite sextet (relative spectral area $S = 54\%$), a very broad sextet (35%, henceforward termed sextet II) and a doublet (11%). In fitting this spectrum, the area ratio of outer lines to middle lines to inner lines for the broad sextet was forced to equal

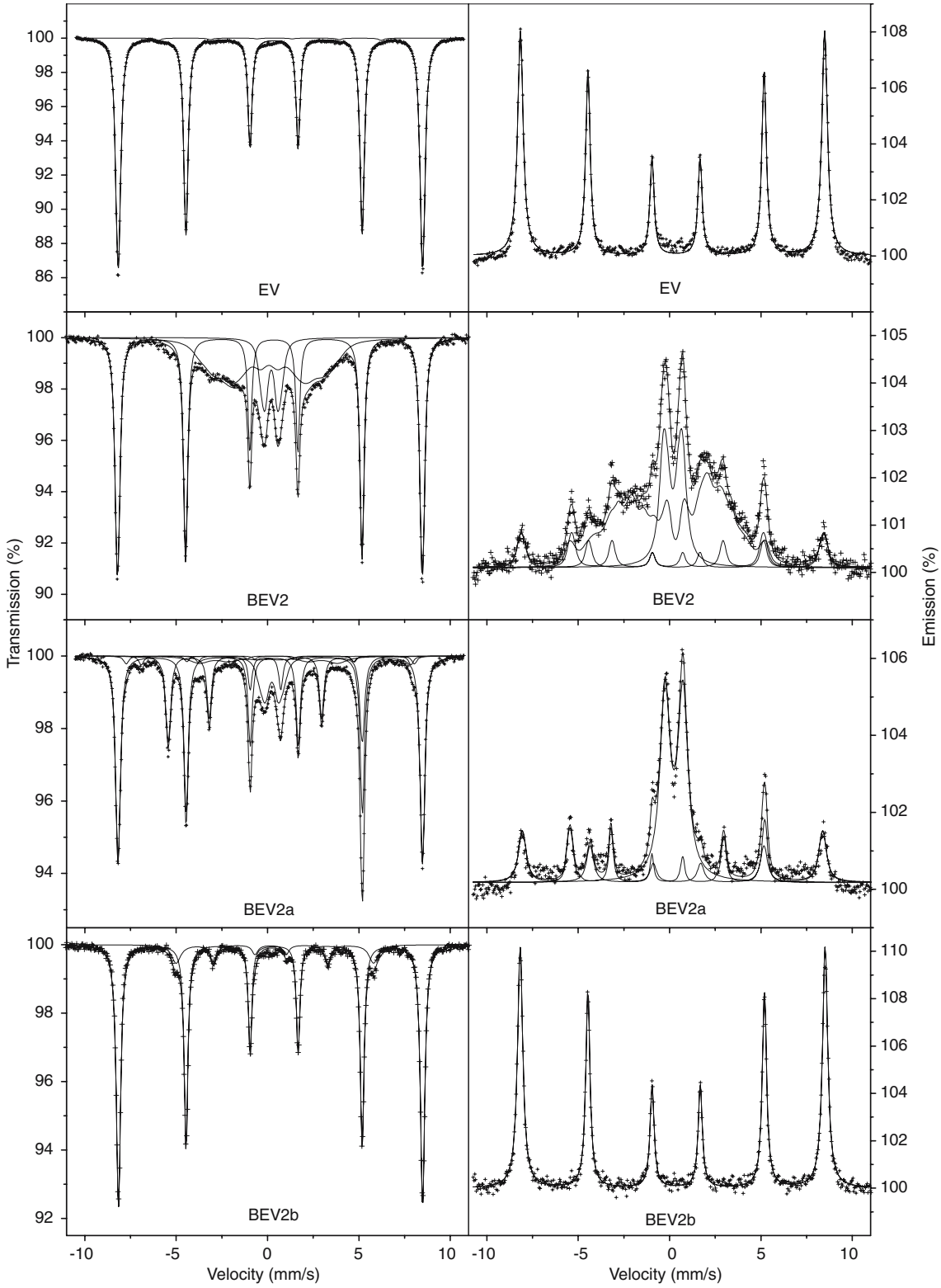

Fig. 4 Room-temperature transmission (left) and ILEEMS (right) Mössbauer spectra

3:2:1. The effect of temperature on the TMS of BEV2 is displayed in Fig. 5 (left) and the numerical results derived from these spectra are listed in Table 2. From these results, it is obvious that sextet II remains considerably broadened, even at 12 K, and that its contribution slightly increases with lowering of

Table 1 Transmission and ILEEMS Mössbauer spectra at room-temperature of the samples studied

	EV				BEV2				BEV2a				BEV2b			
	H_{hf} (kOe)	$2\varepsilon_Q$ (mm/s)	δ (mm/s)	S (%)	H_{hf} (kOe)	$2\varepsilon_Q$ (mm/s)	δ (mm/s)	S (%)	H_{hf} (kOe)	$2\varepsilon_Q$ (mm/s)	δ (mm/s)	S (%)	H_{hf} (kOe)	$2\varepsilon_Q$ (mm/s)	δ (mm/s)	S (%)
Sextet I																
Trans.	517	–0.20	0.37	100	517	–0.21	0.35	54	517	–0.22	0.37	56	516	–0.20	0.37	87
ILEEMS	516	–0.19	0.37	100	515	–0.20[a]	0.37[a]	11	511	–0.25	0.39	23	518	–0.19	0.37	100
Sextet II																
Trans.	–	–	–	–	185	0.00[a]	0.19	35	237	0.00[a]	0.16	7	–	–	–	–
ILEEMS	–	–	–	–	208	0.00[a]	0.24	53	–	–	–	–	–	–	–	–
Sextet III																
Trans.	–	–	–	–	–	–	–	–	329	–0.01	–0.01	22	–	–	–	–
ILEEMS	–	–	–	–	327	0.00[a]	0.00[a]	12	331	0.00	0.00	20	–	–	–	–
Sextet IV/V																
Trans.	–	–	–	–	–	–	–	–	487	0.00[a]	0.26[a]	2	–	–	–	–
									457	0.00[a]	0.58	2				
ILEEMS	–	–	–	–	–	–	–	–	–	–	–	–	–	–	–	–
Sextet VI																
Trans.	–	–	–	–	–	–	–	–	–	–	–	–	335	0.24	0.38	13
ILEEMS	–	–	–	–	–	–	–	–	–	–	–	–	–	–	–	–
Doublet																
Trans.	–	–	–	–	–	0.63	0.31	11	–	0.64	0.35	11	–	–	–	–
ILEEMS	–	–	–	–	–	0.93	0.36	24	–	1.00	0.35	57	–	–	–	–

Isomer shifts are given with reference to metallic iron

Notes: H_{hf} = maximum-probability hyperfine fields; $2\varepsilon_Q$ = quadrupole shifts; δ = isomer shifts; and S = relative areas. For the doublet, $2\varepsilon_Q$ means the quadrupole splitting

[a] Fixed parameter

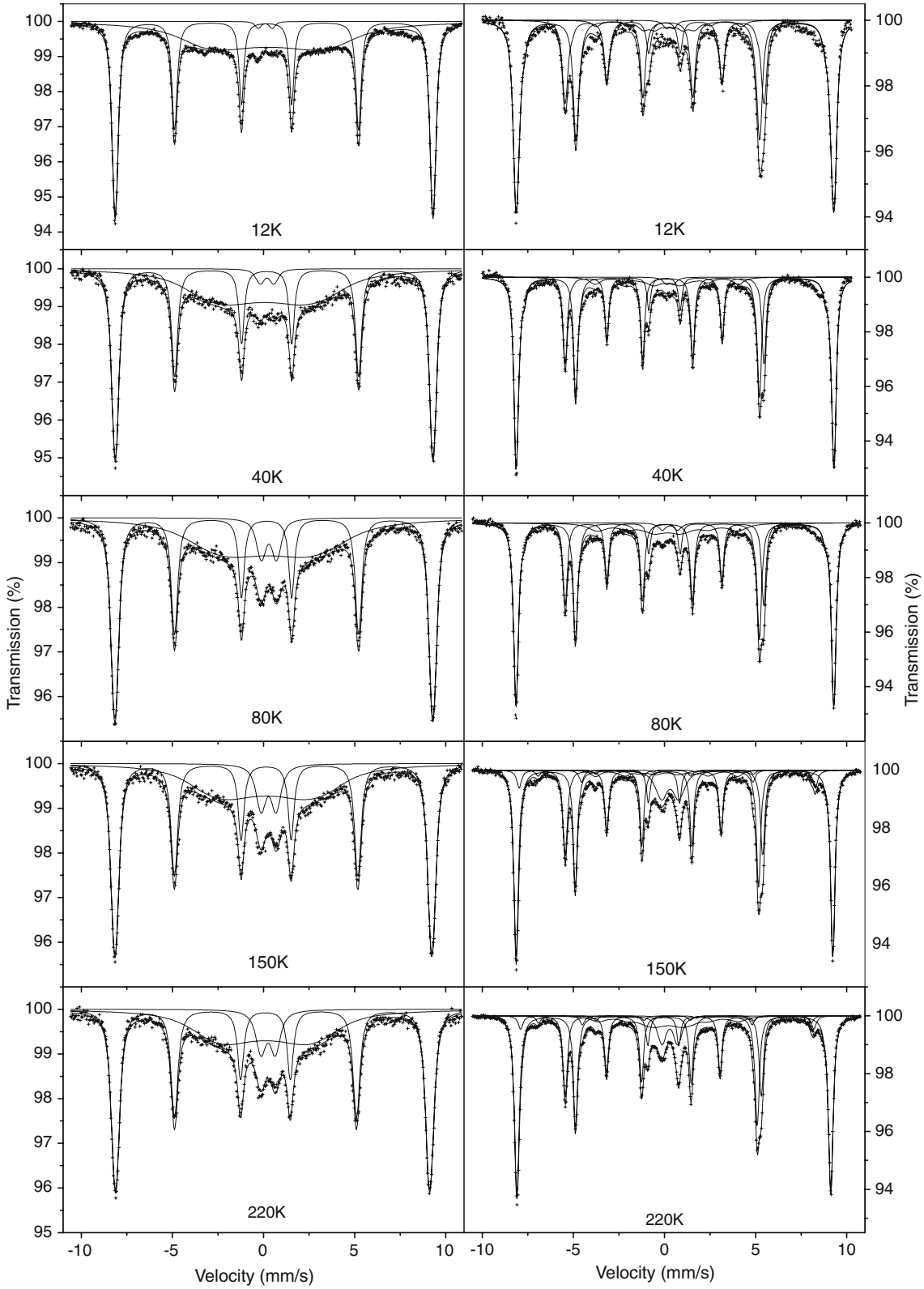

Fig. 5 Temperature dependence of the Mössbauer spectra of samples BEV2 (left) and BEV2a (right)

Table 2 Mössbauer results of samples BEV2 and BEV2a at selected temperatures

Hematite (sextet I)					α-Fe (sextet III)			Magnetite (sextets IV/V)			Sextet II			Doublet		
T (K)	$2\varepsilon_Q$ (mm/s)	H_{hf} (kOe)	S (%)	δ (mm/s)	H_{hf} (kOe)	S (%)	δ (mm/s)	H_{hf} (kOe)	S (%)	δ (mm/s)	H_{hf} (kOe)	S (%)	δ (mm/s)	ΔE_Q (mm/s)	S (%)	δ (mm/s)
BEV2																
12	0.41	541	53	0.48	–	–	–	–	–	–	225	46	0.35	0.78	1	0.20
40	0.41	540	52	0.49	–	–	–	–	–	–	215	45	0.35	0.61	3	0.30
80	0.40	540	50	0.48	–	–	–	–	–	–	213	43	0.35	0.76	7	0.40
150	0.40	537	53	0.45	–	–	–	–	–	–	203	39	0.27	0.81	9	0.39
220	0.39	532	53	0.41	–	–	–	–	–	–	172	38	0.22	0.74	9	0.36
RT	–0.21	517	54	0.35	–	–	–	–	–	–	185	35	0.19	0.63	11	0.31
BEV2a																
12	0.38	542	64	0.50	339	27	0.11	–	–	–	249	8	0.35	0.39	1	0.41[a]
40	0.41	541	64	0.49	338	26	0.11	–	–	–	245	9	0.23	0.39	1	0.41[a]
80	0.41	541	61	0.48	338	24	0.11	–	–	–	240	14	0.28	0.84	2	0.41[a]
150	0.41	539	53	0.45	336	24	0.08	504	5	0.36[a]	241	6	0.16	0.88	10	0.43
								464	2	0.73[a]						
220	0.41	534	53	0.42	334	22	0.04	499	4	0.32[a]	239	9	0.17	0.84	9	0.41
								464	3	0.67						
RT	–0.22	517	56	0.37	329	22	–0.01	487	2	0.26[a]	237	7	0.16	0.64	11	0.35
								457	2	0.58						

Isomer shifts are given with reference to metallic iron

Notes: H_{hf} = maximum-probability hyperfine fields; $2\varepsilon_Q$ = quadrupole shifts; δ = isomer shifts; and S = relative areas. For the doublet, $\Delta\varepsilon_Q$ means the quadrupole splitting

[a] Fixed parameter

temperature. As for the doublet, it seems to persist down to temperatures as low as 12 K, but it is quite possible that it would completely vanish on further lowering the temperature towards 0 K. Due to the weak contribution of this doublet, its Mössbauer parameters are ill defined and the adjusted hyperfine-parameter values inevitably are uncertain, thus explaining the unreal fluctuations in the obtained temperature variations of these values. It is believed, though, that the consistent decrease of the doublet's relative area with decreasing temperature (see Table 2), the amount by which fully accounting for the increase of the area of sextet II, is not unreal.

The above-mentioned findings suggest that sextet II and doublet, as resolved from the TMS spectra of BEV2, both are due to one and the same structural phase of which the magnetic order–disorder transition temperature is spread out over a very broad temperature range. Such behaviour one may expect to be observed for magnetic small-particle or amorphous systems with a broad distribution in particle size or composition, respectively. Based upon published data referring to amorphous Fe–B alloys [4], upon the type of elements present in the starting mixture and upon the observation that no diffraction lines other than those from α-Fe_2O_3 and α-Fe are obvious, one may assign sextet II and doublet to an amorphous, boron-rich Fe–B alloy, henceforward referred to as the a-(Fe,B) phase. The composition of this phase as determined by chemical analysis is $Fe_{0.91}B_{0.09}$.

Finally, the $2\varepsilon_Q$ data for the hematite sextet indicate that the Morin transition of the hematite phase occurs at a temperature well above 220 K, implying a high degree of crystallinity of the parent ferric oxide with minor or no substitutions of the ferric cations by other species such as Al, Mn, Ti, etc. [10], which are common in natural hematites.

The ILEEMS spectrum of BEV2 at RT shows that the amount of hematite in the surface layers, as quantified by the relative spectral area $S = 11\%$ of the hematite component appearing in the ILEEMS, is much less than in the bulk, where $S = 54\%$. On the other hand, the area of doublet has nearly doubled from 11% (bulk) to 24% (surface). Two other components are clearly identified in this ILEEMS spectrum: the broad sextet (53%) corresponding to sextet II in the TMS spectra and a third sextet, designated as sextet III in Table 1, which obviously is attributable to metallic iron (12%). The observation that both sextet II and doublet components in the ILEEMS spectrum are enhanced with respect to their respective counterparts in the TMS spectrum, is consistent with the suggestion that they are attributable to the same constituent, which thus is most likely initially formed in the surface layers of the hematite grains.

The XRD patterns of the samples obtained by heating BEV2 at 400 °C (BEV2a, highly magnetic) and 800 °C (BEV2b, non-magnetic) are reproduced in Fig. 2c and d, respectively. The most noticeable aspect is the presence of a sharp peak corresponding to metallic iron in BEV2a, and the absence of this peak upon heating at 800 °C. Additional diffraction lines, due to magnetite, Fe_3O_4, and B_2O_3 in sample BEV2a

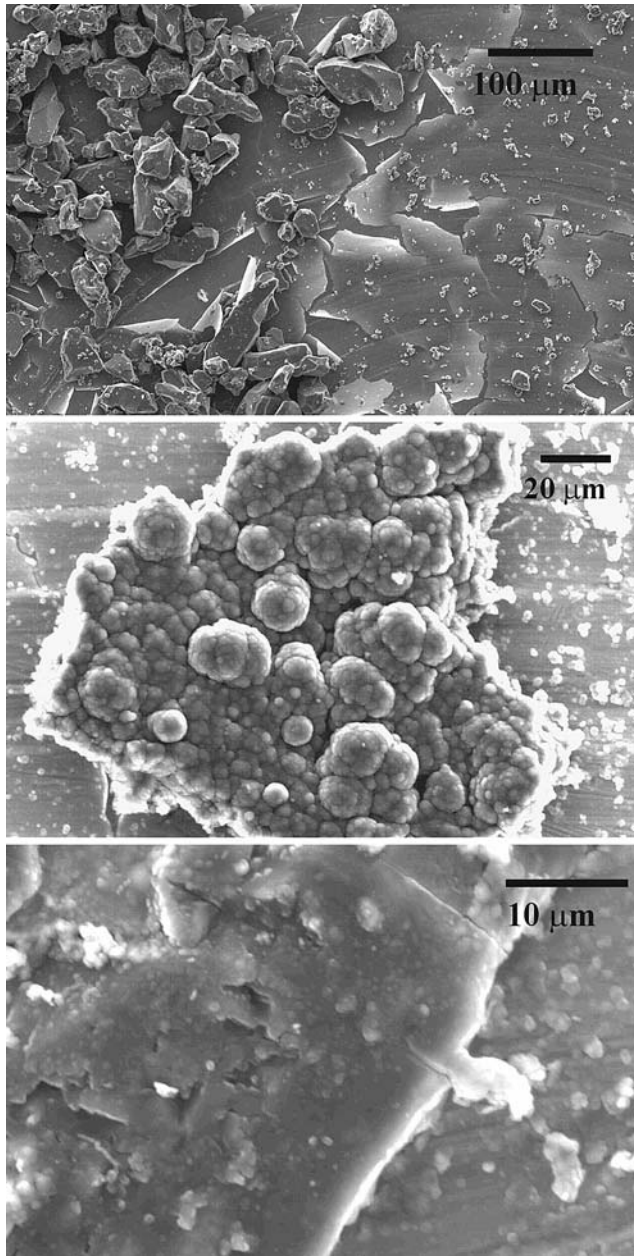

Fig. 6 Scanning electron microscopy images of samples EV (top), BEV2 (middle) and BEV2a (bottom)

and to $FeBO_3$ and B_2O_3 in BEV2b, are readily recognized.

The TGA trace of BEV2a is similar to that of BEV2, except for the absence of the minor gain in mass near 440 °C observed for the latter. The exothermic gain in mass in the range 600–700 °C is almost the same as that observed for BEV2, indicating that the thermal treatment at 400 °C caused no alteration of the phase present in BEV2 that accounts for the withdrawal of mass from the surrounding atmosphere, i.e., most likely of oxygen atoms. After being heated at 800 °C, this phase naturally has vanished. The mass losses reflected in the TGA curves near 100 °C, and associated with sharp endothermic peaks in the DSC curves, for both BEV2a and BEV2b are likely due to removal of moisture adsorbed on the surfaces of the B_2O_3 grains. This oxide is indeed known to be highly hygroscopic.

The TMS spectra of BEV2a (see Figs. 4 and 5) clearly show the presence of α-iron and magnetite, Fe_3O_4, (sextets III and IV/V, respectively, in Tables 1 and 2) along with hematite and the iron phases that give rise to the broad sextet II and a weak doublet. The fraction of the total Fe atoms that forms the hematite phase has remained unchanged from that in the parent sample BEV2 prior to heating. In contrast, the contribution of sextet II to the total spectrum of BEV2a, i.e., ~10%, is considerably lower as compared to BEV2. Its Mössbauer parameters are ill defined and consequently, as one can notice from the data in Table 2, they bear a large scatter for the various temperatures. Remarkably, the relative area of the doublet has remained unaffected by the heating at 400 °C, and as for BEV2 tends to zero when the temperature lowers towards 0 K. Further, the amount of metallic Fe has doubled as a result of the heating.

The TMS of Fe_3O_4 below its Verwey-transition temperature (≈130 K for pure species) is very complicated and up to nine components have been used considered in the past to describe the observed spectral line shapes [11]. In the present study, no attempts were made to include the (weak) magnetite component in the numerical analyses of the TMS spectra recorded at temperatures of 80 K and beneath. As a result of this approximation and of the fact that the hyperfine parameters of the various magnetite sub-spectra are closest to those of hematite, the presence of magnetite is predominantly absorbed by the spectral contribution associated to α-Fe_2O_3. Consequently, the hematite fractions, as determined from the low-temperature TMS spectra, are overestimated and a sudden drop of the relative area S in lowering the temperature from 150 K to 80 K (see Table 2) is evident. In interpreting the TMS spectra in the range 150 K to RT, the magnetite component was taken explicitly into account in the fitting model. However, constraints were required to achieve convergence of the iteration with reasonable parameter values, and it was chosen to force the isomer shifts of the two magnetite sub-spectra to be equal to the values found for a pure, synthetic species [12].

The ILEEMS spectrum of BEV2a (see Fig. 4) shows a predominant contribution from the doublet. As for BEV2, the hematite fraction in the surface layers is less

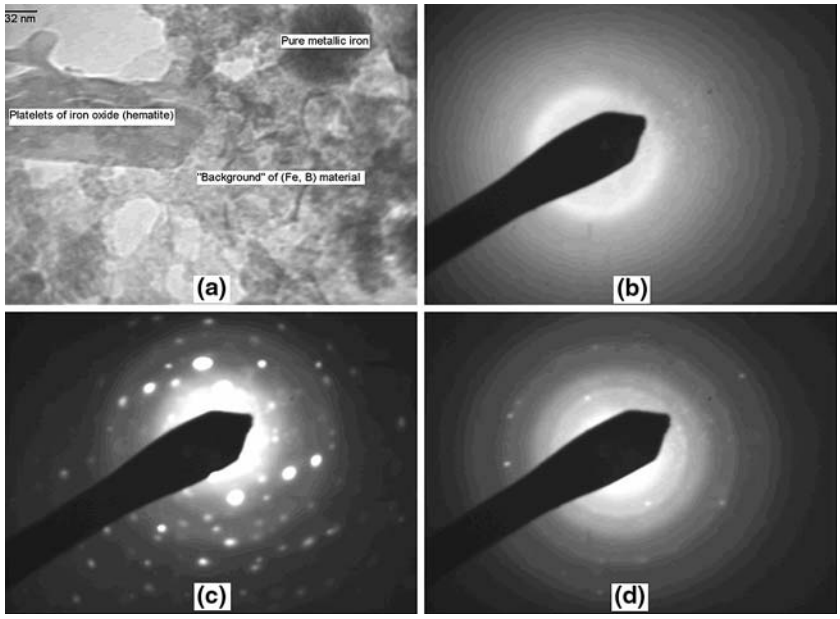

Fig. 7 Transmission electron microscopy and selected-area electron-diffraction images of sample BEV2

than that in the bulk, whilst no difference in that respect is observed for the metallic-Fe fraction. An additional component that would correspond to the sextet II in the TMS spectra and a magnetite contribution are not resolved.

Both the transmission and ILEEMS spectra of BEV2b show the predominant sharp sextet for hematite, but in the transmission data the presence of a second sextet is clearly recognized. Its parameters are similar to those of $FeBO_3$ [13], which is consistent with the XRD pattern of this sample. The borate phase does not appear in the ILEEMS spectrum, implying that the borate grains are embedded in the hematite matrix.

The chemical and subsequent thermal treatments of the iron ore cause a drastic change in the morphology of the particles, as can be seen from SEM images, some of which are reproduced in Fig. 6. The original ore is mainly composed of particles of irregular shape, apparently non-porous and most of which with dimensions around 30 μm. The chemical treatment (BEV2) has produced aggregates of more or less spherical particles with dimensions of the order of 2 μm, whereas subsequent thermal treatment at 400 °C (BEV2a) resulted in the separation of the spherical particles and in the appearance of cavities in the larger particles.

A typical global view of the microstructure of sample BEV2 as observed by TEM is presented in Fig. 7a. It shows the various entities that build up this microstructure. Based on the characteristic X-ray analyses and electron diffraction, they can be identified as: (i) platelets of iron oxide (hematite) with high degree of crystallinity as evidenced by the diffraction image (Fig. 7c), (ii) nodules of pure metallic Fe; electron diffraction (see Fig. 7d) shows these Fe nodules to be amorphous, and (iii) a kind of background of (Fe, B)-containing, poorly crystalline or amorphous material (see electron diffraction image, Fig. 7b). This material is probably the a-($Fe_{0.91}B_{0.09}$) phase identified from the TMS spectra.

Some images referring to the microstructural characterization of the sample BEV2a are reproduced in Fig. 8. The top image (Fig. 8a) shows a micron-sized zone of Fe- and B-containing material. The electron diffraction indicates that the spotted material is amorphous. In addition to these amorphous aggregates, plates consisting of crystalline, sub-micron-sized, more or less spherical Fe-oxide particles are identified. Between the amorphous ($Fe_{0.91}B_{0.09}$)- and crystalline Fe-oxide plates one observes zones of boron-rich material(s). They appear in the images as light-grey areas as illustrated in Fig. 8c. It is suggested that these zones are composed of the B_2O_3 observed in the XRD pattern. Dispersed throughout the whole sample, sharp needles of hematite are noticed, as exemplified by Fig. 8b. These needles have a thickness of less than 10 nm and their long axis exceeds 100 nm. So, the hematite particles present in BEV2a seem to occur in two very different morphologies, i.e., needle-shaped

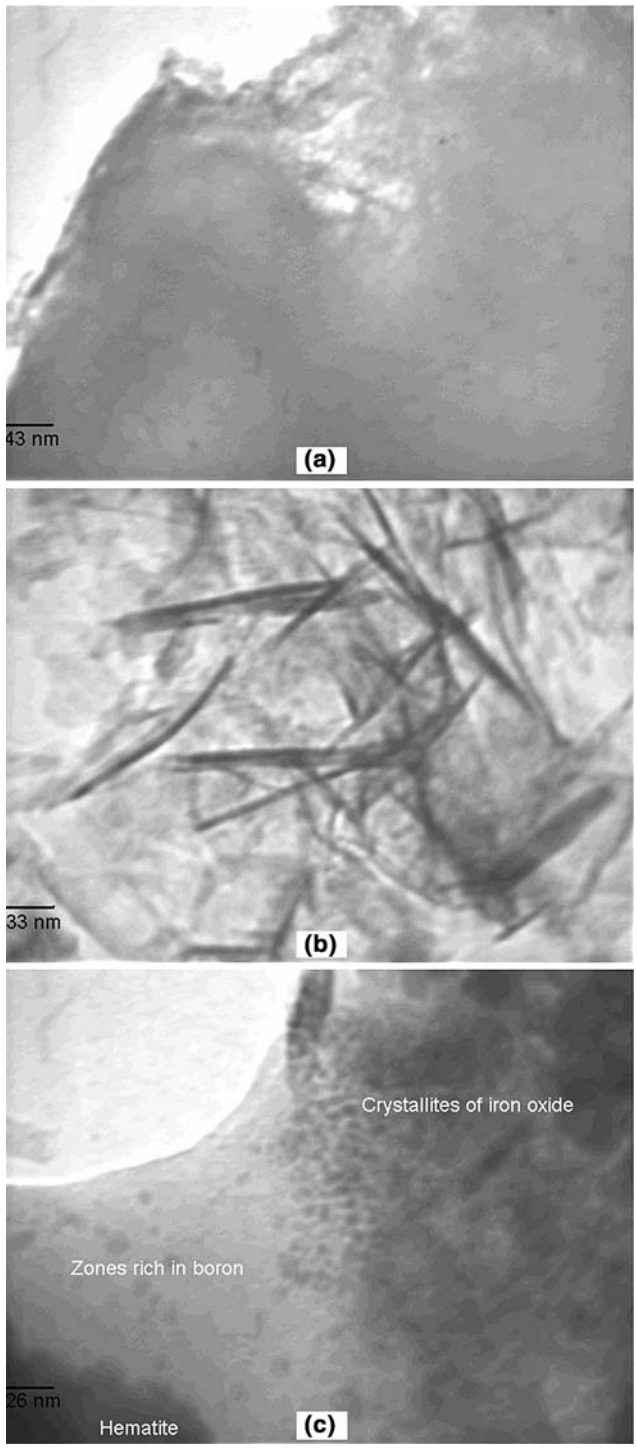

Fig. 8 Transmission electron microscopy images of sample BEV2a

and near spherical. This different morphology apparently does not affect the Mössbauer spectra. Surprisingly, the TEM characterization of BEV2a could not spot any metallic-Fe particles, although both XRD and MS irrefutably indicate their presence.

Combining these TEM observations for BEV2a with the XRD and MS results, it can be inferred that heating at 400 °C of the α-Fe_2O_3–a-($Fe_{0.91}B_{0.09}$) composite powder, has resulted in the crystallization and/or oxidation of more than half of the a-($Fe_{0.91}B_{0.09}$) phase to α-Fe and to Fe_3O_4 and B_2O_3, respectively. Further, the already present superficial, amorphous metallic Fe is converted to α-Fe and the original, plate like morphology of the hematite has changed to a mix of nodular and acicular particles. The formation of Fe_3O_4 and B_2O_3 is reflected in the thermal analyses by the observation of a gain in weight in the TGA curve of BEV2 slightly above 400 °C, which is due to the withdrawal of oxygen from the surrounding atmosphere to form the oxides. The reason why the process according to the TGA recording sets in at a temperature above the static heat treatment at 400 °C is attributable to the rapid heating rate in the TGA experiment and the inertia of the sample to reach equilibrium with the temperature of the surrounding atmosphere.

In conclusion, the amorphous Fe–B alloy and α-Fe formed by chemical reduction of hematite took place only in the surface the particle since that no Fe ions it was present in the solution. Also, the formation of those phases took place on the surface of the hematite covering the grains surface observed and proved by results of the transmission Mössbauer spectroscopy and integral low-energy electron Mössbauer spectroscopy (ILEEMS).

Acknowledgements This work was partially funded by CNPq and Fapemig (Brazil), and by the Fund for Scientific Research—Flanders, Belgium. One of us (V. G. de Resende) thanks the Program Alban, the European Union Programme of High Level Scholarships for Latin America, scholarship No. E04M034189BR.

References

1. Dragieva ID, Stoynov ZB, Klabunde KJ (2001) Script Mater 44:2187
2. Foster GD, Barquín LF, Cohen NS, Pankhurst QA, Parkin IP (1999) J Mater Proc Tech 92–93:525
3. Petit S, David K, Doumerc JP, Grenier JC, Seguelong T, Pouchard M (1998) CR Acad Sci Paris, Série IIc:517
4. Linderoth S, Mørup S (1991) J Appl Phys 69:5256
5. Saida J, Ghafari M, Nakamura Y, Inoue A, Masumoto T (1993) Nuclear Instr Meth Phys Res B76:223
6. Song X, Yusheng X, Huali J, Qing X (1993) Nuclear Instr Meth Phys Res B76:260
7. De Grave E, Vandenberghe RE, Dauwe C (2005) Hyperfine Interact 161:147
8. Forster GD, Barquín LF, Bilsborrow RL, Pankhurst QA, Parkin IP, Steer WA (1999) J Mater Chem 9:2537
9. De Grave E, Vandenberghe RE (1986) Hyperfine Interact 28:643
10. De Grave E, Bowen LH, Vochten R, Vandenberghe RE (1988) J Magn Magn Mater 72:141
11. Vandenberghe RE, De Grave E (1989) In: Long GJ, Grandjean F (eds) Mössbauer spectroscopy applied to inorganic chemistry, vol 3. Plenum Press, New York, p 59
12. Persoons RM (1990) Ph.D. Thesis, University of Gent
13. Bayukov OA, Abd-Elmeguid MM, Ivanova NB, Kazak NV, Ovchinnikov SG, Rudenko VV (2004) Phys Solid State 46(6):1088